Arabian Journal for Science and Engineering (2023) 48:7781–7795
https://doi.org/10.1007/s13369-023-07809-6

RESEARCH ARTICLE-CHEMISTRY

Ecofriendly Maghemite/Halloysite-like Nanotubes Nanocomposite for Highly Efficient Removal of Cd(II) from Industrial Wastewater

Tahany K. Mohamed[1] · Mahmoud F. Mubarak[1] · Mohamed Keshawy[1] · Thanaa Abdel Moghny[1] · Said A. Sayed[2] · Omnia I. Ali[2]

Received: 11 October 2022 / Accepted: 16 February 2023 / Published online: 12 April 2023
© The Author(s) 2023

Abstract
Kaolinite is a widely available and inexpensive substance that has been successfully employed to decontaminate different hazardous contaminants from wastewater by adsorption. In this study, halloysite-like nanotubes (HNTs) were prepared via intercalation followed by ultrasonic rolling of the kaolinite layers. Then, maghemite nanoparticles were co-precipitated within the HNTs matrix to produce a maghemite/HNTs nanocomposite (MG@HNTs). XRD, SEM, TEM, FTIR, and a BET analyzer were used to characterize the MG@HNTs nanocomposite, which was then utilized to eliminate Cd(II) from aqueous solutions (water and wastewater). Using a batch methodology, the impact of various adsorption parameters on Cd(II) removal was explored. MG@HNTs nanocomposite exhibited a high adsorption capacity (q_e) of 264.47 mg g^{-1} for Cd (II). The kinetic data well conformed to pseudo-2nd-order, while the adsorption isotherms conformed to the Langmuir model. The desorption study demonstrated that the MG@HNTs nanocomposite could be successfully regenerated and recycled five times, without losing its original removal efficiency. Furthermore, MG@HNTs exhibited effective implementation to remove cadmium from real water samples, including tap and industrial wastewater. This study confirmed the successful application of MG@HNTs as an efficient, eco-friendly, and sustainable adsorbent at a high level of feasibility for the uptake of hazardous contaminants from industrial wastewater.

Keywords Kaolinite · Intercalation · Halloysite-like nanotubes · Maghemite · Wastewater · Heavy metals

1 Introduction

One of the most important environmental concerns that humanity has faced in recent decades is water contamination. Contamination of water with harmful metal ions like cadmium, as well as heavy metals discharged into aquatic habitats, are both major concerns [1]. It is known that Pb, Co, Cr, Hg, Se, Zn, As, Cd, U, and Ni are toxic metals that are released into the environment in significant quantities, posing major health dangers to humans [2]. These metals, particularly Cd, accumulate in numerous tissues of living creatures and cause a variety of defects and diseases, posing a severe environmental and public health threat [3]. Therefore, novel and contemporary water treatment technologies are being developed worldwide to control the unregulated release of these harmful substances in wastewater in order to decontaminate the environment [4].

Different heavy metals' removal techniques have been designed, including ion exchange, reverse osmosis, membrane filtration, flotation, electrochemical precipitation, evaporation, and adsorption. Several researchers have applied adsorption to get rid of hazardous heavy metals from wastewater in recent years [5–15]. Adsorption is a common technique given that it is simple to use at low concentrations; efficient for harmful pollutants' removal with high capacity and low cost, and environmentally friendly [16–18]. Furthermore, as nanotechnology advances, nanomaterials have been successfully synthesized and have demonstrated higher efficiency and faster adsorption rates for heavy metals than conventional adsorbents [19, 20]. Magnetic nanoparticles are

✉ Tahany K. Mohamed
tahany.kamel2020@gmail.com

✉ Omnia I. Ali
omniaali@science.helwan.edu.eg;
omniaibrahim95@gmail.com

1 Egyptian Petroleum Research Institute (EPRI), Ahmed El-Zomer, Box. No. 11727, Nasr City, Cairo, Egypt

2 Chemistry Department, Faculty of Science, Helwan University, Ain Helwan, Cairo 11792, Egypt

popular among nanomaterials because of their wide range of advanced uses in areas including catalysis, data storage, nano-tagging, adsorption, medicine, ferrofluids, and wastewater treatment [21–25].

Although nanomaterials with magnetic properties have been widely proposed for heavy metal ions removal from wastewater [26, 27], there hasn't been much research on the investigation of maghemite nanoparticles (γ-Fe_2O_3) as heavy metals' adsorbents [28, 29]. Besides, the issue of the instability of magnetic nanoparticles, which leads to agglomeration, has prompted research on hybrid materials [30] to overcome the issues of agglomeration while keeping the special property of magnetism in the new material. In this regard, clay minerals have different active sites, and therefore, they are an excellent candidate for a hybrid with maghemite [31–33].

Clay minerals are a type of hydrous aluminosilicate with a sheetlike structure and very small particle size, less than two microns. Clay minerals, especially natural clays, were employed as efficient adsorbents because of their porosity, high surface area, cation exchange capacity, acidity, surface electrical charge, and many types of active sites. Kaolinite is a clay mineral that comprises tetrahedral sheets (SiO_4) and octahedral sheets ($AlO_2(OH)_4$) of the 1:1-type. It is a potent adsorbent that has been recently used in several studies to remove diverse types of contaminants [34, 35]. Also, the clay minerals with tubular structures at the nanoscale, as halloysite ($Al_2(OH)_4Si_2O_5.2H_2O$), have attracted the interest of adsorption experts [36, 37]. The primary form of halloysite found in nature is the nanoscale tubular halloysite, which is a polymorph of kaolinite that is hydrated and holds a water molecules' layer between the aluminosilicate layers [38].

Generally, multilayer aluminosilicate nanoscrolls can be produced by rolling clay material layers under appropriate intercalation, delamination, and ultrasonic scrolling [39, 40]. The synthesis of halloysite-like nanoscrolls from platy kaolinite has been investigated by many researchers [41–44]. These nanoscrolls exhibit a wide range of properties and morphologies that make them beneficial substitutes for halloysite nanotubes [45]. Halloysite has a one-of-a-kind one-dimensional mesoscopic/macroscopic porous structure; therefore, it has been applied to different applications [46, 47].

Herein, halloysite-like nanotubes (HNTs) were prepared via intercalation followed by ultrasonication rolling of kaolinite layers. The current method for HNTs preparation consumes less time and less electricity than the previous reported methods [40, 48, 49]. Then, the physicochemical characteristics of the prepared HNTs were enhanced through the loading of maghemite nanoparticles (MG) using the co-precipitation method. To the best of the authors' knowledge, it is the first time to prepare magnetic halloysite-like nanotubes nanocomposite using maghemite nanoparticles to be applied to wastewater treatment. The novel prepared nanocomposite (MG@HNTs) was employed to remove cadmium ions as a model pollutant from aqueous solutions (water and wastewater). Incorporation of maghemite nanoparticles is expected to enhance the physicochemical characteristics of the halloysite-like nanotubes. Versatile techniques were employed to characterize the prepared materials. In addition, the adsorption kinetics, isotherms, thermodynamics, and reusability were also explored. Here, the prepared MG@HNTs nanocomposite outperformed many other composite materials in the Cd(II) decontamination process.

2 Experimental Methods

2.1 Materials

Natural kaolinite powder was supplied by Morgan Chemical Ind (Egypt). Cetrimonium bromide (CTAB) was purchased from MP Biomedicals, Inc. (France). Methanol (MeOH), ethanol (EtOH), and dimethyl formamide (DMF) were from Piochem for Laboratory Chemicals (Egypt). Ferric chloride ($FeCl_3.6H_2O$) was supplied by Spectrum Chemical MFG Corp (Egypt), and ferrous sulfate ($FeSO_4.7H_2O$) and cadmium nitrate ($Cd(NO_3)_2$) were procured from Eisen-Golden (Egypt).

2.2 Procedures

2.2.1 Intercalation of Kaolinite and Preparation of Halloysite-like Nanotubes (HNTs)

Kaolinite (10–20 g) was treated with distilled water (500 mL) to remove surface impurities. This procedure was carried out six times in a row in order to remove all contaminants. The suspension was centrifuged for 10 min after each wash. Finally, kaolinite drying was carried out in a drying oven at 100 °C for two days.

To prepare the DMF-intercalated kaolinite [50], 25 g of kaolinite was blended with 200 mL of DMF solution (10% H_2O: 90% DMF, *v/v*) under constant stirring for around 24 h. The formed fine particles were collected by centrifugation and washed repeatedly with methanol to remove extra DMF. The hybrid material (Ka/DMF) produced by intercalating the kaolinite layers with DMF was dried at 60 °C for 24 h. After that, to produce the methoxy kaolinite [51], 10 g of Ka/DMF was dissolved in 200 mL of MeOH and stirred at 100 ºC for 12 h. The suspension was centrifuged and then dried at 60 °C for 24 h.

To produce HNTs, 1.0 g of methoxy kaolinite was blended with CTAB in a 50 mL MeOH solution and stirred for 48 h at ambient temperature. Then, to complete the rolling of aluminosilicate sheets and to generate HNTs, the combination

was treated with ultrasonication for around 4 h. The resultant aluminosilicate nanotubes (HNTs) were gathered using centrifugation, washed extensively with distilled water and ethanol five times to eliminate any surfactant excess, and then dried for 24 h at 80 °C. Lastly, the formed HNTs were calcined at 300 °C for two hours to eliminate any surfactant contamination.

2.2.2 Preparation of Maghemite/Halloysite-like Nanotubes Nanocomposite (MG@HNTs)

The chemical co-precipitation technique was utilized to prepare maghemite/halloysite-like nanotubes nanocomposite (MG@HNTs). First, magnetite/halloysite-like nanotubes nanocomposite (Mag/HNTs) was prepared according to the procedures proposed by Xu et al. with some modifications [52]. In brief, HNTs were added to a solution of ferric chloride and ferrous sulfate with a molar ratio of 2:1 for n Fe^{3+} to n Fe^{2+} and agitated for 20 min at 298 K to generate a stable suspension. The temperature was then raised to 353 K. After that, ammonia solution was added drop by drop to adjust the pH to (9–10), causing iron oxide to precipitate, and the stirring was continued for 1 h. Finally, the prepared Mag/HNTs sample was washed using distilled water and EtOH, and dried under a vacuum for 24 h at 333 K, followed by calcination at 573 K for 2 h to form maghemite/ halloysite-like nanotubes nanocomposite (MG@HNTs).

2.3 Characterization

XRD patterns of kaolinite, HNTs, maghemite, and MG@HNTs nanocomposite were examined with a D8 Focus X-ray diffractometer (Bruker, Germany) with CuKα radiation ($\lambda = 0.154$ nm, 40 kV, 40 mA) in a scan range (2θ) of 5° to 75°. The FTIR spectra of the prepared samples were reported on a Perkin-Elmer IR spectrophotometer in the range of 400–4000 cm^{-1}. Transmission electron microscopy (TEM) images were picked up with a JEM-2100 microscope (JEOL, Japan). The samples' surface morphology was investigated by scanning electron microscopy (Zeiss SEM Ultra 60). The specific surface area and pore characteristics were estimated employing the BET method (BET model BELSORP, BEL Master—Ver 7.1.0.0, MicrotracBEL, Corp). The size distribution was estimated through the BJH method.

2.4 Cadmium Uptake Studies

The batch equilibrium approach was applied to conduct the adsorption experiments. In particular, 50 mL of Cd(II) was mixed with 0.025 g of MG@HNTs using a thermally controlled shaker at a speed of 200 rpm. The initial pH impact on Cd(II) adsorption onto MG@HNTs was investigated at different pH levels (2–7) with shaking for 2 h at room temperature. The solutions' pH was changed by adding drops of 0.1 mol L^{-1} HCl and/or 0.1 mol L^{-1} NaOH. By mixing MG@HNTs with aqueous solutions of Cd(II) at various time intervals, the contact time infleunce on the Cd(II) removal efficiency using MG@HNTs was evaluated. In addition, the change in the removal efficiency with the variation of the initial Cd(II) concentration (10 to 200 mg L^{-1}) was studied. Also, different masses (0.025, 0.05, 0.1, 0.2, 0.4, and 0.5 g) of MG@HNTs were shaken with Cd(II) solutions while keeping the other parameters constant to examine how the used adsorbent mass affects the removal behavior. Cd(II) adsorption was also tested at various temperatures in the range of 25 to 65 °C. After the MG@HNTs nanocomposite had been removed after each adsorption test, the solution was separated by centrifugation and filtered using Whatman filter paper. The remaining Cd(II) concentration was determined by an AA-7000 atomic absorption spectrophotometer (Shimadzu, Japan).

The Cd(II) ions uptake by MG@HNTs (q_e) in mg g^{-1} can be estimated as follows:

$$q_e = \frac{V(C_o - C_e)}{m} \tag{1}$$

where V refers to the volume of solution (L), C_o: initial cadmium concentration (mg L^{-1}), C_e: the remaining Cd(II) concentration (mg L^{-1}) at equilibrium in solution, and the MG@HNTs mass is m (g). The percentage of removal using MG@HNTs is represented as:

$$\text{Removal efficiency}(\%) = \frac{C_o - C_e}{C_o} \times 100 \tag{2}$$

2.5 Regeneration and Reusability Studies

Before performing the desorption experiments, Cd-loaded-MG@HNTs were first washed many times with distilled water to eliminate any Cd(II) ions that were not strongly bonded to the nanocomposite surface. To carry out the regeneration procedure, 0.2 g of Cd-loaded-MG@HNTs that were loaded with 10 mg L^{-1} Cd(II) were shaken with a solution of 0.01 mol L^{-1} HCl (50 mL) for an hour at a speed of 200 rpm at room temperature. Equation (3) was used to estimate the desorption efficiency (%) as follows:

$$\text{Desorption efficiency}(\%) = \frac{\text{Amount of released Cd(II) ions}}{\text{Amount of sorbed Cd(II) ions}} \times 100 \tag{3}$$

Reusability was achieved by employing the regenerated MG@HNTs nanocomposite in the subsequent adsorption

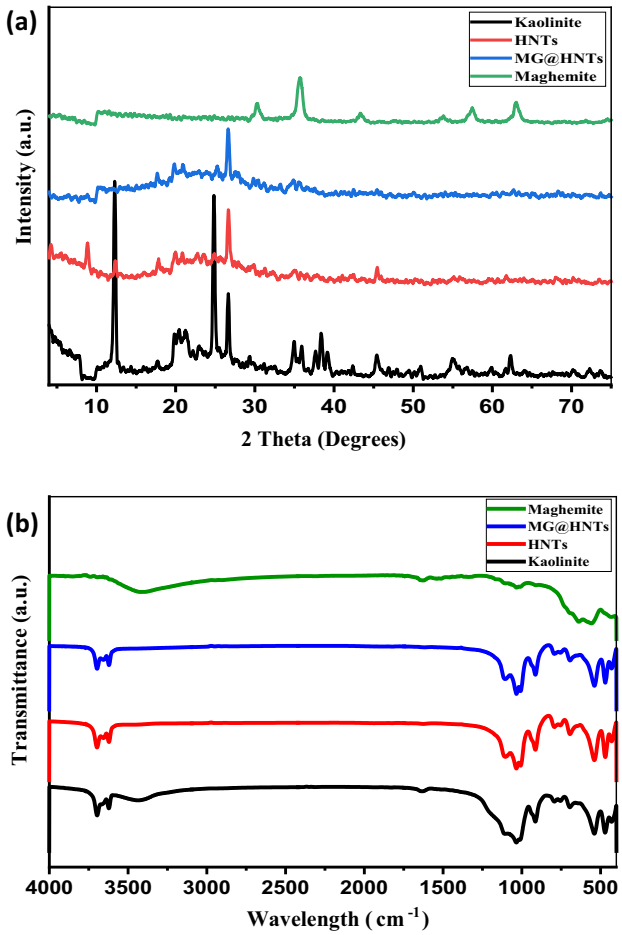

Fig. 1 XRD patterns (**a**) and FTIR spectra (**b**) of kaolinite, HNTs, maghemite, and MG@HNTs nanocomposite

experiments and repeating the adsorption–desorption technique several times with the same adsorbent sample. The MG@HNTs sample was washed extensively with distilled water before drying; therefore, it could be used again in the next cycle.

3 Results and Discussion

3.1 Characterization Results

3.1.1 Crystalline and Structural Properties

The structural properties and quantitative analysis of the maghemite, kaolinite, HNTs, and MG@HNTs nanocomposite were studied based on the XRD technique as displayed in Fig. 1a. Natural kaolinite is highly crystalline, and its diffraction peaks were detected at 2-theta of 12.33°, 24.82°, 26.65°, and 38.37°, which were attributable to the crystallographic planes of (0 0 1), (0 0 2), (1 1 1), and ($\bar{2}$ 0 2), respectively [40, 53, 54]. The basal spacing of the major diffraction peak of kaolinite was determined to be 0.72 nm. As shown in Fig. 1a, the evidence for the intercalation and elimination of molecules between the interlayers of kaolinite was provided by a reduction in the intensity of the main d_{001} basal diffraction of kaolinite with a maximum of $d = 0.717$ nm.

In the HNTs sample, the (001) kaolinite reflection still exists but at a very low intensity, and a new diffraction peak for HNTs appears at $2\theta = 8.87$ ($d_{001} = 0.99$ nm). The d_{001} value in this work is 0.99 nm, which is larger than that of some previous reports [40, 55, 56]. In addition, the basal reflections emerged at 0.99 and 0.72 nm, indicating the presence of residual untransformed kaolinite [57]. On the other side, after the maghemite nanoparticles' incorporation into the HNTs sample, the reflections of the HNTs that were discovered in the MG@HNTs pattern had a very small shift and their intensities decreased.

Figure 1a also shows the XRD pattern of the nanocrystalline maghemite (γ-Fe_2O_3) structure. Typical peaks detected at 2θ of 30.26°, 35.66°, 43.34°, 53.78°, 57.38°, and 62.96° were indexed to the crystal planes of (2 2 0), (3 1 1), (4 0 0), (4 2 2), (5 1 1), and (4 4 0), respectively (JCPDS card no. 39–1346) [58, 59].

3.1.2 Functional Chemical Properties

Figure 1b shows the FTIR spectra of kaolinite, HNTs, maghemite, and MG@HNTs nanocomposite throughout a frequency range of 4000–400 cm^{-1}. In kaolinite, the peaks at 3697, 3655, and 3622 cm^{-1} exhibited the characteristic –OH stretching. The peaks at 3697 and 3653 cm^{-1} were assigned to the stretching of the outer Al–OH groups, while the one at 3622 cm^{-1} was due to the inner Al–OH groups stretching [60, 61]. The wide peak at 3438 cm^{-1} and the one at 1633 cm^{-1} were assigned to the stretching and bending vibrations of the –OH groups of the physically adsorbed water molecules, respectively [61]. Also, the Si–O stretching in the tetrahedral sheet was indicated by the strong peaks at 1035 and 471 cm^{-1} [62]. The observed peak at 914 cm^{-1} was assigned to stretching of Al-Al–OH functional groups in the octahedral layer, which is characteristic of the kaolinite structure [56]. In addition, the peaks at around 695 and 539 cm^{-1} corresponded to the Si–O-Al structure stretching [56].

As shown in Fig. 1b, the primary kaolinite peaks in the HNTs spectrum after intercalation and sonication of kaolinite were slightly displaced from their locations, and their intensities were seen to be slightly less than those of kaolinite [56]. After the incorporation of maghemite nanoparticles, the FTIR spectrum of the MG@HNTs nanocomposite exhibited no significant changes within HNTs. However, the intensity of the peak at 541 cm^{-1} slightly increased due to the stretching vibration of Fe–O functional groups [58, 63]. On the other hand, the broad peak around 3417 cm^{-1} seen in the

maghemite spectrum indicated the presence of the OH groups [63], which disappeared in the MG@HNTs nanocomposite.

3.1.3 Morphological Properties

SEM and TEM images (Fig. 2) were utilized to describe the structural morphology of kaolinite, HNTs, and MG@HNTs nanocomposite. Figure 2a, d reveals the high crystalline nature of kaolinite crystals that had a plate-like shape with a pseudo-hexagonal structure of 0.5–2 μm in size. After the processes of intercalation and ultrasonication rolling, the kaolinite layers were transformed into nanotubes (tabular nanoscrolls), which revealed the successful delamination and folding of the layers of kaolinite (Fig. 2b, e). Also, the images of HNTs showed some uncurled kaolinite sheets. Figure 2e clearly demonstrates the formation of HNTs with typical cylindrical shapes. Moreover, the TEM image showed that the nanotubes had an average diameter ranging from 70–200 nm and the length of the cylinders ranged from 0.5–2.7 μm. The structural morphology of the MG@HNTs nanocomposite was revealed by the SEM and TEM images (Fig. 2c, f). As shown in Fig. 2c, the synthesized nanocomposite had a brighter surface due to the occurrence of maghemite particles that covered the surface.

3.1.4 Surface Area and Pore Size Analysis

The N_2 adsorption isotherms and pore size distribution of kaolinite, maghemite, HNTs, and MG@HNTs are illustrated in Figs. S1 and S2. The nitrogen isotherm for kaolinite in Fig. S1 (a) shows a Type II isotherm, which is indicative of the presence of abundant macropores [38]. Also, the samples of HNTs and MG@HNTs still show Type II isotherms (Fig. S1(b,c)). This may be due to the presence of uncurled kaolinite sheets, as previously observed in TEM images (Fig. 2e, f). On the other hand, the isotherm of maghemite showed a Type IV (Fig. S1(d)), indicating the presence of abundant mesopores and a high gas adsorption capacity. Fig. S2 shows the BJH pore size distribution curves of kaolinite, maghemite, HNTs, and MG@HNTs. As noticed, kaolinite, HNTs, and MG@HNTs nanocomposite have pores spanning from micropores to macropores. In contrast, maghemite had pores inside, which were mainly mesopores.

Table 1 displays the values of the specific surface area (SSA) and porosity characteristics of maghemite, kaolinite, HNTs, and MG@HNTs nanocomposite. As observed, the SSA of kaolinite increased after the intercalation, exfoliation, and ultrasonication processes, where the SSA increased from 8.34 $m^2\ g^{-1}$ for kaolinite to 10.95 $m^2\ g^{-1}$ for HNTs. In the MG@HNTs nanocomposite, it can be seen that with the maghemite nanoparticles' incorporation into the HNTs matrix, the SSA also increased. The observed increase in the SSA with the maghemite nanoparticles' inclusion was possibly because of the partial intercalation of maghemite in the clay layers, thus creating new interlayer porosity [64]. The increase in the SSA of MG@HNTs is expected to be beneficial for adsorption. Moreover, it can be noted that the decline in the pore volume of MG@HNTs compared to that of HNTs was due to the maghemite nanoparticles being introduced into the HNTs matrix.

3.2 Cadmium Uptake Studies

3.2.1 Comparison Between the Prepared Samples for Cd(II) Removal

Figure 3a shows an assessment of the removal efficiency of kaolinite, maghemite, HNTs, and MG@HNTs nanocomposite for Cd(II) removal under the same circumstances: 0.05 g MG@HNTs, 100 mg L^{-1} Cd(II), pH 6, 4 h of contact time, and temperature of 25 °C. The removal efficiency of MG@HNTs nanocomposite for Cd(II) ions was the highest among the other samples. This is due to the fact that MG@HNTs nanocomposite combines the features of both maghemite and HNTs. Moreover, maghemite nanoparticles were consistently distributed on the surface of MG@HNTs, as revealed from TEM results, which also increases the adsorption capability of the nanocomposite. Therefore, MG@HNTs nanocomposite was selected as an optimal adsorbent for the subsequent studies.

3.2.2 Impact of Initial pH

One of the vital factors that regulates the adsorption process is pH. The influence of solution pH (2–7) on the Cd(II) adsorption using MG@HNTs was investigated as shown in Fig. 3b. The value of pHpzc for MG@HNTs was evaluated (Fig S3) using batch equilibrium method [65], and it was found to be 6.5. It was noticed that cadmium ions have adsorption in the pH range of 2 to 7, where the adsorption reached a plateau at pH 6. In the highly acidic media (pH = 2), Cd(II) adsorption was relatively low due to competition for binding sites of MG@HNTs nanocomposite between the excess protons and Cd(II) cations. However, as pH increased from 3 to 7, the surface charge of the MG@HNTs nanocomposite became more negatively charged. Therefore, as the pH of solutions increased, the competition between Cd(II) ions and protons was limited, and the electrostatic attraction between the negatively charged MG@HNTs surface and the positively charged Cd(II) ions was enhanced, resulting in the rise of Cd(II) adsorption. Consequently, pH 6 was utilized as the optimum pH in the subsequent experiments. Based on the pHpzc value and these observations, the electrostatic interaction was not the exclusive mechanism for Cd(II) adsorption

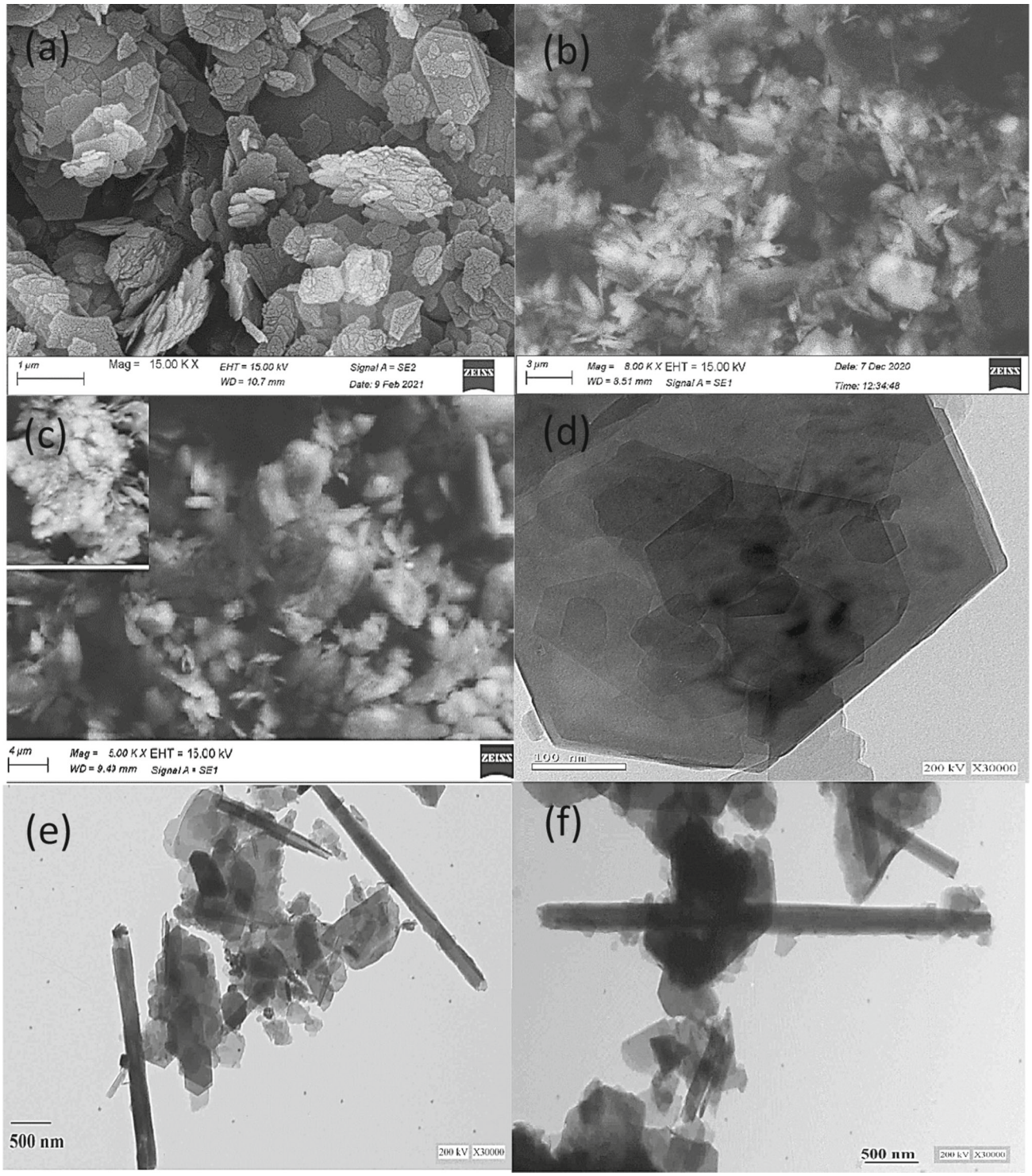

Fig. 2 SEM images of kaolinite (**a**), HNTs (**b**), and MG@HNTs nanocomposite (**c**); and TEM images of kaolinite (**d**), HNTs (**e**), and MG@HNTs nanocomposite (**f**)

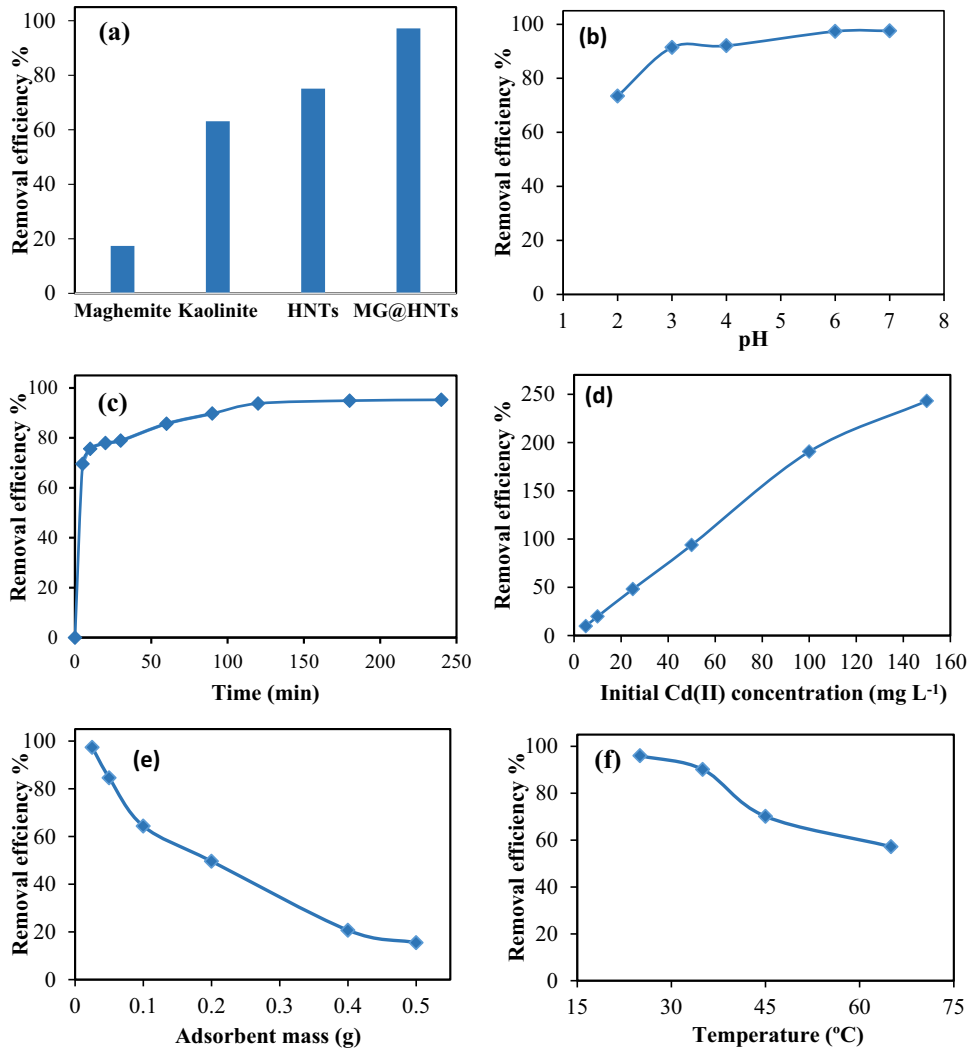

Fig. 3 Comparison between the different prepared samples for Cd(II) removal (pH 6, 100 mg L^{-1} Cd(II), 0.05 g MG@HNTs, 2 h, 25 °C) (**a**), and impact of adsorption parameters on Cd(II) removal using MG@HNTs: initial pH (**b**), contact time (**c**), initial Cd(II) concentration (**d**), MG@HNTs mass (**e**), and temperature (**f**)

Table 1 Porosity characteristics and BET surface areas of the prepared materials

Materials	Total pore volume (cm^3 g^{-1})	Mean pore diameter (nm)	SSA (m^2 g^{-1})
Maghemite	0.3099	16.52	75.05
Kaolinite	0.0769	36.88	8.34
HNTs	0.1007	36.81	10.95
MG@HNTs	0.1065	32.94	12.94

by MG@HNTs, and it is possible that a variety of sorption processes (electrostatic attraction, surface complexation, ion-exchange, and co-precipitation) were involved in Cd(II) removal. Wang et al. (2022) reported similar results for Cd(II) removal.

3.2.3 Impact of Contact Time

To investigate the contact time impact, 0.025 g of MG@HNTs was contacted with a 50 mL solution of 100 mg L^{-1} Cd(II) ions at different time intervals at pH 6. The results for the Cd(II) adsorption are demonstrated in Fig. 3c. The results revealed that the removal efficiency of Cd(II) using MG@HNTs raised as the contact time increased, until it reached equilibrium after 120 min. The data indicated that adsorption was rapid at the beginning, with more than 75% of Cd(II) ions were adsorbed within 10 min, and then the adsorption became much slower with the progress of time till equilibrium was achieved. This could be because the adsorption active sites on the MG@HNTs surface were being depleted. As observed, the Cd(II) adsorption onto MG@HNTs attained equilibrium after 120 min. Therefore, the rest of experiments have been run for 120 min, which was the optimal time for Cd(II) removal.

3.2.4 Impact of Initial Cd(II) Concentration

Figure 3d shows the impact of Cd(II) concentration on the adsorption capacity using MG@HNTs nanocomposite, which was explored at different concentrations (5, 10, 25, 50, 100, and 150 mg L^{-1}) using 0.025 g MG@HNTs at pH 6 and 2 h of contact time. It was found that as the initial Cd(II) concentration increased, so did the capacity of uptake. When the Cd(II) concentration rose from 5 to 150 mg L^{-1}, the uptake capacity increased from 10 to 243 mg g^{-1}. This may be attributed to the diffusion of Cd(II) ions from the solution phase to the MG@HNTs' surface due to the increase in the driving force of Cd(II) ions, promoted by the rise in the Cd(II) concentration. As a consequence, the collisions between Cd(II) ions and the MG@HNTs' surface improved, and thereby the uptake capacity increased in accordance with Abdelbasir et al. [66].

3.2.5 Impact of Adsorbent Mass

Adsorption is significantly impacted by the mass of adsorbent utilized. Figure 3e depicts the impact of MG@HNTs mass on the Cd(II) removal efficiency. The removal percentage decreased significantly with the rise in the MG@HNTs nanocomposite mass. This might be ascribed to a reduction in the overall adsorption surface area available for Cd(II) ions' binding as a consequence of the aggregation or overlapping of the adsorption binding sites caused by the excessive number of MG@HNTs particles [67, 68]. Therefore, 0.025 g of MG@HNTs was chosen as the optimal MG@HNTs mass for all other experiments.

3.2.6 Impact of Temperature

The temperature impact on the Cd(II) adsorption using MG@HNTs is shown in Fig. 3f. In this study, the temperature was ranging from 25 to 65ºC under the conditions of 50 mL of 100 mg L^{-1} of Cd(II) at pH 6, 2 h of contact time, and 0.025 g of MG@HNTs. The figure showed that the Cd(II) removal efficiency using MG@HNTs decreased with the rise of temperature.

3.3 Adsorption Isotherms

In this study, the most common adsorption isotherm models were adopted to determine the fraction of Cd(II) at equilibrium that reached the adsorbent and solution phases. The equilibrium data of the Cd(II) removal using MG@HNTs were investigated using Freundlich, Langmuir, Dubinin-Radushkevich (D-R), and Temkin isotherm models.

According to the Freundlich isotherm, adsorbents have heterogeneous surfaces with a variety of adsorption potential sites. The linearized Freundlich isotherm model [69] can be represented as:

$$\log q_e = \frac{1}{n} \log C_e + \log \ K_f \tag{4}$$

where q_e is the adsorption capacity (mg g^{-1}) at equilibrium, the Freundlich constant is K_f (mg g^{-1}), and the adsorption intensity is ($1/n$). A straight line was fitted to the data by plotting log q_e vs. log C_e (Fig. 4). The values of K_f and n are illustrated in Table 2, where a value of ($1 < n < 10$) indicated a favorable adsorption of Cd(II) onto MG@HNTs [70].

The Langmuir isotherm, on the contrary, implies that adsorption occurs as a continuous monolayer of adsorbate molecules covering homogenous sites on the adsorbent's surface [71], implying that once an adsorbate occupies a site, no additional adsorption can occur at that occupied site. The Langmuir isotherm is expressed by Eq. 5 [72]:

$$\frac{C_e}{q_e} = \frac{C_e}{q_{max}} + \frac{1}{q_{max} K_L} \tag{5}$$

where q_{max} is the maximum Cd(II) adsorption capacity (mg g^{-1}) and K_L is the Langmuir constant. By plotting C_e/q_e versus C_e, the values of q_{max} and K_L can be estimated (Fig. 4 and Table 2). As seen in the table, the Langmuir model's correlation coefficient (R^2) value was larger than that of the Freundlich model, demonstrating that the Langmuir model was correlated with the obtained experimental data. This implied that monolayer adsorption was taking place and that the surface of the prepared MG@HNTs was homogeneous in nature.

R_L is a dimensionless constant ($R_L = 1/(1 + K_L \ C_o)$) that may be used to describe the features of the Langmuir equilibrium model. A favorable Cd(II) adsorption process onto MG@HNTs was demonstrated by the obtained value of R_L ($0 < R_L < 1$) (Table 2).

The D-R model isotherm is a generalized version of the Langmuir type [73]. The linearized D-R model equation may be expressed as follows:

$$\ln(q_e) = \beta\varepsilon^2 + \ln(q_{DR}) \tag{6}$$

where the D-R optimum monolayer adsorption capacity is denoted by q_{DR} (mg g^{-1}), the activity coefficient with respect to the mean adsorption energy is β (mol^2 kJ^{-2}), and ε is the Polanyi potential that has the following relationship with the equilibrium concentration:

$$\varepsilon = RT \ln\left[1 + \frac{1}{C_e}\right] \tag{7}$$

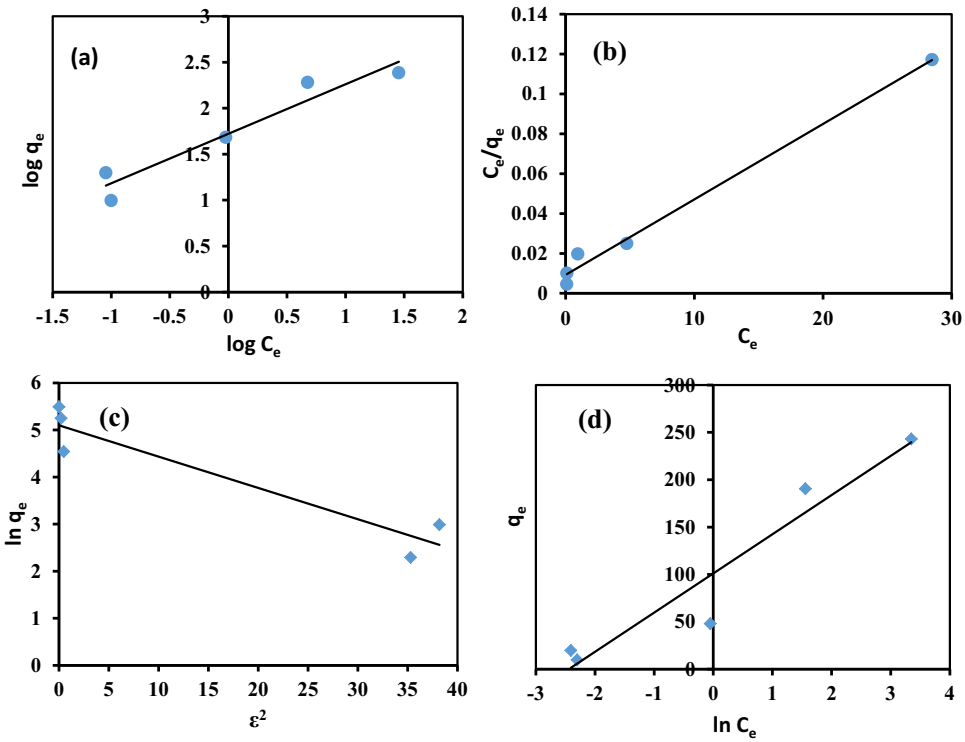

Fig. 4 Adsorption isotherms for Cd(II) removal using MG@HNTs: Freundlich model (**a**), Langmuir model (**b**) (D-R) model (**c**), and Temkin model (**d**)

T is the temperature (K), and R is the gas constant (8.3145 J K^{-1} mol^{-1}). The next formula is used for the estimation of the mean adsorption energy (E).

$$E = (2\beta)^{-0.5} \tag{8}$$

Figure 4 displays the plot of ln q_e versus ε^2 for Cd(II) adsorption on MG@HNTs, while Table 2 displays the estimated values of D-R parameters. As demonstrated, the value of E was < 8, indicating that physisorption dominated Cd(II) adsorption onto MG@HNTs [74].

Temkin model isotherm considers the consequences of interactions between adsorbates and adsorbents on the adsorption process. Equation (8) gives the Temkin isotherm's expression [75].

$$q_e = \frac{RT}{b_T} \ln K_T + \frac{RT}{b_T} \ln C_e \tag{9}$$

where b_T is correlated with the adsorption heat (kJ mol^{-1}), and K_T is a constant (L g^{-1}). The q_e vs. ln (C_e) plot for Cd(II) ions adsorption using MG@HNTs with a slope of (RT/b_T) and intercept of ((RT/b_T) ln K_T) is demonstrated in Fig. 4. Table 2 displays the K_T and b_T values. The b_T value was < 20 kJ mol^{-1}, which is distinctive of weak electrostatic interactions [76]. Therefore, the Cd(II) adsorption onto MG@HNTs was consistent with the physisorption process.

Table 2 The estimated parameters of the examined isotherm models for Cd(II) removal using MG@HNTs

Isotherm model	Parameters	Values
Freundlich	K_f (mg g^{-1})	52.64
	n	1.86
	R^2	0.9269
Langmuir	K_L (L mg^{-1})	0.406
	q_{max} (mg g^{-1})	264.47
	R^2	0.9909
	R_L	0.016
Dubinin–Radushkevich (D–R)	β	6.66×10^{-2}
	q_{DR}	164.16
	E (kJ mol^{-1})	2.74
	R^2	0.8929
Temkin	K_T	11.53
	b_T (kJ mol^{-1})	0.06
	R^2	0.9221

3.4 Adsorption Kinetics

The kinetics of Cd(II) adsorption using MG@HNTs were investigated. The rate of reactions between Cd(II) ions and active sites of MG@HNTs was described by the pseudo-1st-order, the pseudo-2nd-order, and intra-particle diffusion

Table 3 The estimated parameters of the examined kinetic models for Cd(II) removal using MG@HNTs

Kinetics model	Parameters	Values
Pseudo-1st-order	k_1	0.024
	$q_{e\,(exp)}$ (mg g^{-1})	190.5
	q_e (mg g^{-1})	63.11
	R^2	0.9753
Pseudo-2nd-order	k_2	0.001
	$q_{e\,(exp)}$ (mg g^{-1})	190.5
	q_e (mg g^{-1})	193.9
	R^2	0.9994
Intra-particle diffusion	k_i	5.136
	C	131.27
	R^2	0.9811

models. The pseudo-1st-order model as given by the Lagergren model as follows [77].

$$\log(q_e - q_t) = \log q_e - (k_1 t/2.303) \tag{10}$$

The pseudo-2nd-order can also be written in a linearized form:

$$\frac{t}{q_t} = \frac{1}{K_2 q_e^2} + \frac{t}{q_e} \tag{11}$$

where q_t is the adsorption capacity (mg g^{-1}) at any time interval (t), k_1 is the pseudo-1st-order rate constant (min^{-1}), and k_2 is the pseudo-2nd-order rate constant (g mg^{-1} min^{-1}). The graphs of log ($q_e - q_t$) versus time and t/q_t versus time were plotted as demonstrated in Fig. 5b. Furthermore, the constants' values are tabulated in Table 3.

A pseudo-2nd-order model is more acceptable, based on the R^2 values, for a better description of the kinetiecs of Cd(II) adsorption onto MG@HNTs.

3.4.1 Intra-Particle Diffusion Model

The intra-particle diffusion model [78] was used to fit the kinetic experimental results using Eq. (12).

$$q_t = k_i t^{0.5} + C \tag{12}$$

The intra-particle diffusion rate constant (g mg^{-1} min$^{-0.5}$) is k_i, while the intercept is C (mg g^{-1}), which represents the boundary layer thickness. The intercept and slope of the plot of q_t versus $t^{0.5}$ can be used to estimate k_i and C values (Fig. 5c). The plot showed two stages without passing through the origin point, which suggested that the intra-particle diffusion was not the only rate-determining stage to control the Cd(II) adsorption onto MG@HNTs. The first stage corresponded to surface adsorption, where the ions of Cd(II) diffused from the solution to the MG@HNTs' surface, and the second stage expressed the penetration of Cd(II) ions into the inner pores of MG@HNTs.

3.5 Thermodynamic Parameters

The mechanism of adsorption processes at different temperatures was explored through thermodynamic quantities, including changes in Gibbs free energy (ΔG), change in entropy (ΔS), and change in enthalpy of adsorption (ΔH). To determine the ΔG, ΔH, and ΔS values for the Cd(II) adsorption using MG@HNTs, the following equations were used [68]:

$$\ln K_d = \frac{\Delta S}{R} - \frac{\Delta H}{RT} \tag{13}$$

$$\Delta G = \Delta H - T\Delta S \tag{14}$$

The dissociation constant (K_d) was estimated from ($K_d = q_e/C_e$) and the plot of ln K_d versus $1/T$ was determined to be linear as shown in Fig. 5d. The values of ΔH and ΔS were estimated from the slope and intercept of the Van't Hoff plot (Eq. 13), respectively. A list of the estimated thermodynamic parameters is provided in Table 4.

The decrease in K_d with the rise in the temperature implied that the Cd(II) adsorption onto MG@HNTs was exothermic in nature. Also, the negative values of ΔG indicated the spontaneity of the Cd(II) adsorption. Also, it can be noticed that less negative values of ΔG were attained with the rise in temperature, demonstrating that the Cd(II) adsorption onto MG@HNTs was suppressed at higher temperatures. The negative value of ΔH was an indication of the typical exothermic adsorption process. In addition, the negative value of ΔS inferred that during the Cd(II) adsorption, the randomness degree at the MG@HNTs/solution interface decreased.

3.6 Regeneration and Reusability Studies

Regeneration is a critical step since it affects the effectiveness, capacity, and cost of developing adsorbents for wastewater treatment [79]. To investigate the regeneration possibility, the desorption process was studied using 0.01 mol L^{-1} HCl as the desorption solution. The amount of desorbed Cd(II) was quantified and the desorption efficiency for Cd-loaded-MG@HNTs was estimated using Eq. (3). The reusability of MG@HNTs was checked for several cycles, and the findings are illustrated in Fig. 6. As demonstrated, MG@HNTs can be reused for Cd(II) elimination, with a promising capacity for five cycles and a slight reduction in capacity as the number of regeneration processes increases.

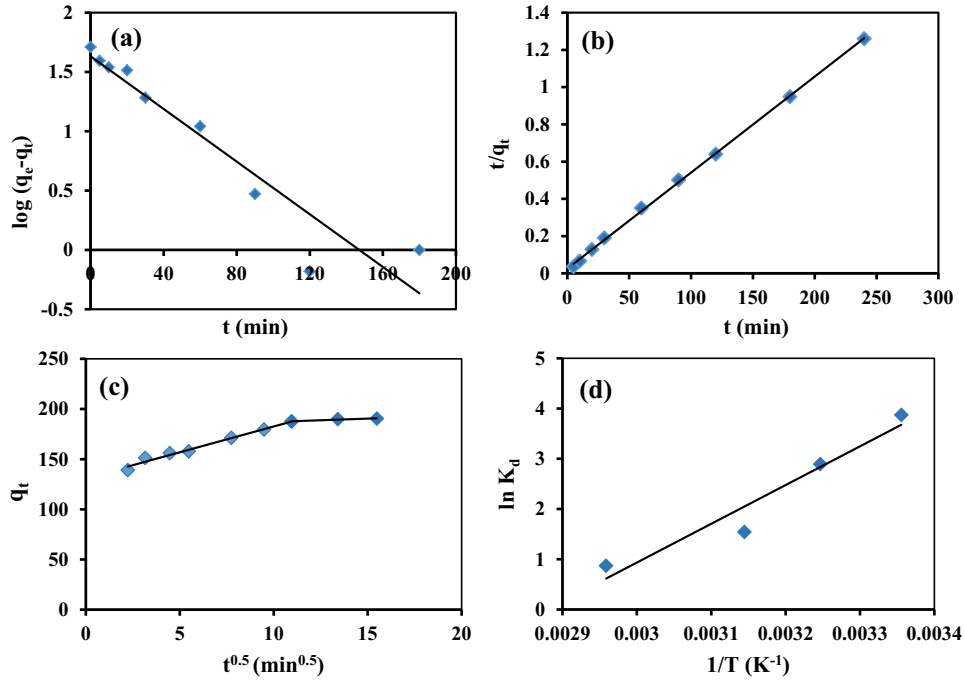

Fig. 5 Kinetic models: pseudo-1st-order (**a**), pseudo-2nd-order (**b**), intra-particle diffusion (**c**), and thermodynamics plot (**d**) for Cd(II) removal using MG@HNTs

Table 4 The estimated thermodynamic parameters for Cd(II) removal using MG@HNTs

T (K)	K_d	ΔG (kJ mol^{-1})	ΔH (kJ mol^{-1})	ΔS (J mol^{-1} K^{-1})
298	48.00	− 9.10	− 64.06	− 184.42
308	18.03	− 7.26		
318	4.68	− 5.42		
338	2.38	− 1.73		

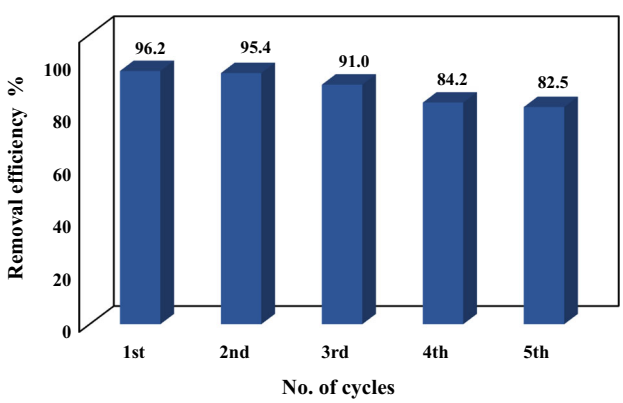

Fig. 6 Reusability of MG@HNTs nanocomposite for Cd(II) removal

To ensure the stability of MG@HNTs nanocomposite, the XRD pattern of Cd-loaded-MG@HNTs after the regeneration process was recorded (Fig. S4). The figure clarifies that the XRD pattern of the regenerated MG@HNTs was almost the same as that of the original MG@HNTs, indicating the MG@HNTs' stability.

3.7 Applications for Real Samples

Finally, the prepared nanocomposite was tested for its analytical usefulness in decontaminating Cd(II) ions from various types of water samples, including tap water and industrial wastewater (Emessa factory, East Nile, Beni Suef). The decontamination of Cd(II) from water samples was inspected by contacting a 50 mL aliquot containing MG@HNTs mass of 0.05 g at the optimum pH for 1 h. To assess the selectivity of the prepared MG@HNTs for Cd(II) removal, the concentrations of other metal ions in the tested industrial wastewater sample were measured. In this regard, Pb(II) and Co(II) coexisted with Cd(II) at concentrations of 13.33 and 15.72 mg L^{-1}, respectively. The tap water sample was spiked with 10 mg L^{-1} of Cd(II). The effectiveness of MG@HNTs as an efficient adsorbent to decontaminate cadmium ions from real samples is shown in Table 5. The obtained results demonstrated the selectivity and feasibility of MG@HNTs to decontaminate real water samples from Cd(II).

Table 5 Cd(II) removal from real water samples using MG@HNTs

Water samples	Cd(II), mg L^{-1}		Removal %
	Before treatment	After treatment	
Industrial wastewater	36.3	1.78	95.1
Tap water	10.0	0.34	96.6

Table 6 A comparison of uptake capacities of MG@HNTs with different adsorbents

Adsorbent	q_{max} (mg g^{-1})	References
Iron oxide nanoparticles	167.36	[80]
Pectin–iron oxide magnetic nanocomposite	48.99	[81]
Kaolinite nanotubes	116.3	[40]
Kaolin	41.84	[82]
MnO-kaolinite	36.47	[83]
Unmodified kaolinite	12.58	[84]
APMS-MMT nanoclay	143.32	[85]
Zero valent iron graphene composites	134	[86]
Acid-modified kaolinite	114	[87]
Nanocomposite material (CPM)	186.36	[88]
DMTD grafted mesoporous silica	167.33	[89]
DPDB immobilized mesoporous silica	176.19	[90]
MG@HNTs	264.47	This study

3.8 Comparison with Other Adsorbents

The estimated q_{max} for the Cd(II) adsorption using MG@HNTs is compared to other adsorbents as shown in Table 6. The information in the table reflected the high uptake adsorption capacity of MG@HNTs nanocomposite in comparison with many other adsorbents. This can be primarily attributed to the alteration of kaolinite sheets into nanotubes and the maghemite nanoparticles' incorporation as well. Furthermore, the significant adsorption capacity was most likely due to the abundance of functional groups on the MG@HNTs surface, which provided more surface adsorption sites for Cd(II) uptake.

4 Conclusion

In this study, the physicochemical characteristics of a locally abundant kaolinite clay as an adsorbent were enhanced by producing halloysite-like nanotubes, which were combined with the extraordinary properties of maghemite nanoparticles to produce an eco-friendly and low-cost sorbent with high adsorption capacity for wastewater treatment. The prepared maghemite/halloysite-like nanotubes nanocomposite (MG@HNTs) has been characterized and applied to remove Cd(II) ions from wastewater. Variable parameters affecting the adsorption process were explored. The optimal pH for Cd(II) removal was pH 6 with a maximum adsorption capacity of 264.47 mg g^{-1}. MG@HNTs offered an outstanding improvement for Cd(II) decontamination process when compared to other composite materials. The experimental data correlated with the pseudo-2nd-order kinetics and the Langmuir isothermal model. Further, the values of ΔG were negative, suggesting that Cd(II) adsorption using MG@HNTs occurred spontaneously. MG@HNTs had a five-cycle Cd(II) removal capacity and can decontaminate real samples with high selectivity from Cd(II). In summary, the findings of this study proved the effective use of MG@HNTs for wastewater treatment as an eco-friendly and sustainable adsorbent.

Supplementary Information The online version contains supplementary material available at https://doi.org/10.1007/s13369-023-07809-6.

Acknowledgements The authors are appreciative of the funding provided for this research by the Academy of Scientific Research & Technology (ASRT), as represented by the Scientists for Next Generation Scholarship (ASRT-SNG).

Funding Open access funding provided by The Science, Technology & Innovation Funding Authority (STDF) in cooperation with The Egyptian Knowledge Bank (EKB).

Declarations

Conflict of interest All authors declare that there are no competing personal or financial interactions that may have impacted the study described in this publication).

Open Access This article is licensed under a Creative Commons Attribution 4.0 International License, which permits use, sharing, adaptation, distribution and reproduction in any medium or format, as long as you give appropriate credit to the original author(s) and the source, provide a link to the Creative Commons licence, and indicate if changes were made. The images or other third party material in this article are included in the article's Creative Commons licence, unless indicated otherwise in a credit line to the material. If material is not included in the article's Creative Commons licence and your intended use is not permitted by statutory regulation or exceeds the permitted use, you will need to obtain permission directly from the copyright holder. To view a copy of this licence, visit http://creativecommons.org/licenses/by/4.0/.

References

1. El-Safty, S.A.; Shenashen, M.; Ismael, M.; Khairy, M.; Awual, M.R.: Optical mesosensors for monitoring and removal of ultra-trace concentration of Zn (II) and Cu (II) ions from water. Analyst **137**, 5278–5290 (2012)
2. Dey, M.; Akter, A.; Islam, S.; Chandradey, S.; Choudhury, T.R.; Fatema, K.J.; Begum, B.A.: Assessment of contamination level pollution risk and source apportionment of heavy metals in the Halda River water Bangladesh. Heliyon **7**, e08625 (2021)
3. Arshad, M.N.; Sheikh, T.A.; Rahman, M.M.; Asiri, A.M.; Marwani, H.M.; Awual, M.R.: Fabrication of cadmium ionic sensor based on (E)-4-Methyl-N′-(1-(pyridin-2-yl) ethylidene) benzenesulfonohydrazide (MPEBSH) by electrochemical approach. J. Organomet. Chem. **827**, 49–55 (2017)
4. Ma, Y.; Ran, D.; Shi, X.; Zhao, H.; Liu, Z.: Cadmium toxicity: a role in bone cell function and teeth development. Sci. Total Environ. **769**, 144646 (2021)
5. Shrestha, R.; Ban, S.; Devkota, S.; Sharma, S.; Joshi, R.; Tiwari, A.P.; Kim, H.Y.; Joshi, M.K.: Technological trends in heavy metals removal from industrial wastewater: a review. J. Environ. Chem. Eng. **9**, 105688 (2021)
6. Kumar, P.S.; Gayathri, R.; Rathi, B.S.: A review on adsorptive separation of toxic metals from aquatic system using biochar produced from agro-waste. Chemosphere **285**, 131438 (2021)
7. Awual, M.R.; Hasan, M.M.; Islam, A.; Rahman, M.M.; Asiri, A.M.; Khaleque, M.A.; Sheikh, M.C.: Introducing an amine functionalized novel conjugate material for toxic nitrite detection and adsorption from wastewater. J. Clean. Prod. **228**, 778–785 (2019)
8. Awual, M.R.: Assessing of lead (III) capturing from contaminated wastewater using ligand doped conjugate adsorbent. Chem. Eng. J. **289**, 65–73 (2016)
9. Awual, M.R.; Islam, A.; Hasan, M.M.; Rahman, M.M.; Asiri, A.M.; Khaleque, M.A.; Chanmiya Sheikh, M.: Introducing an alternate conjugated material for enhanced lead(II) capturing from wastewater. J. Clean. Prod. **224**, 920–929 (2019)
10. Awual, M.R.; Hasan, M.M.; Asiri, A.M.; Rahman, M.M.: Cleaning the arsenic(V) contaminated water for safe-guarding the public health using novel composite material. Compos. B Eng. **171**, 294–301 (2019)
11. Awual, M.R.: Ring size dependent crown ether based mesoporous adsorbent for high cesium adsorption from wastewater. Chem. Eng. J. **303**, 539–546 (2016)
12. Awual, M.R.; Hasan, M.M.: A ligand based innovative composite material for selective lead(II) capturing from wastewater. J. Mol. Liq. **294**, 111679 (2019)
13. Islam, M.A.; Angove, M.J.; Morton, D.W.; Pramanik, B.K.; Awual, M.R.: A mechanistic approach of chromium (VI) adsorption onto manganese oxides and boehmite. J. Environ. Chem. Eng. **8**, 103515 (2020)
14. Islam, M.A.; Awual, M.R.; Angove, M.J.: A review on nickel(II) adsorption in single and binary component systems and future path. J. Environ. Chem. Eng. **7**, 103305 (2019)
15. Awual, M.R.: A novel facial composite adsorbent for enhanced copper (II) detection and removal from wastewater. Chem. Eng. J. **266**, 368–375 (2015)
16. Chakraborty, R.; Asthana, A.; Singh, A.K.; Jain, B.; Susan, A.B.H.: Adsorption of heavy metal ions by various low-cost adsorbents: a review. Int. J. Environ. Anal. Chem. **102**, 342–379 (2022)
17. Awual, M.R.; Hasan, M.M.; Iqbal, J.; Islam, M.A.; Islam, A.; Khandaker, S.; Asiri, A.M.; Rahman, M.M.: Ligand based sustainable composite material for sensitive nickel(II) capturing in aqueous media. J. Environ. Chem. Eng. **8**, 103591 (2020)
18. Hasan, M.N.; Salman, M.S.; Islam, A.; Znad, H.; Hasan, M.M.: Sustainable composite sensor material for optical cadmium(II) monitoring and capturing from wastewater. Microchem. J. **161**, 105800 (2021)
19. Awual, M.R.: Solid phase sensitive palladium(II) ions detection and recovery using ligand based efficient conjugate nanomaterials. Chem. Eng. J. **300**, 264–272 (2016)
20. Awual, M.R.: Novel nanocomposite materials for efficient and selective mercury ions capturing from wastewater. Chem. Eng. J. **307**, 456–465 (2017)
21. Pouran, S.R.; Bayrami, A.; Aziz, A.A.; Daud, W.M.A.W.; Shafeeyan, M.S.: Ultrasound and UV assisted Fenton treatment of recalcitrant wastewaters using transition metal-substituted-magnetite nanoparticles. J. Mol. Liq. **222**, 1076–1084 (2016)
22. Belachew, N.; Devi, D.R.; Basavaiah, K.: Facile green synthesis of l-methionine capped magnetite nanoparticles for adsorption of pollutant Rhodamine B. J. Mol. Liq. **224**, 713–720 (2016)
23. Iconaru, S.L.; Guégan, R.; Popa, C.L.; Motelica-Heino, M.; Ciobanu, C.S.; Predoi, D.: Magnetite (Fe_3O_4) nanoparticles as adsorbents for As and Cu removal. Appl. Clay Sci. **134**, 128–135 (2016)
24. Fouda, A.; Hassan, S.E.-D.; Saied, E.; Azab, M.S.: An eco-friendly approach to textile and tannery wastewater treatment using maghemite nanoparticles (γ-Fe_2O_3-NPs) fabricated by Penicillium expansum strain (Kw). J. Environ. Chem. Eng. **9**, 104693 (2021)
25. Al-Hakkani, M.F.; Gouda, G.A.; Hassan, S.H.: A review of green methods for phyto-fabrication of hematite (α-Fe_2O_3) nanoparticles and their characterization, properties, and applications. Heliyon **7**, e05806 (2021)
26. Kumar, S.: Carbon based nanomaterial for removal of heavy metals from wastewater: a review. Int. J. Environ. Anal. Chem. (2021). https://doi.org/10.1080/03067319.2021.1977930
27. Kumar, S.; Jain, S.; Lamba, B.Y.: A review on synthesis, characterisation and surface modification of magnetic nanoparticle and its composite for removal of heavy metals from wastewater. Int. J. Environ. Anal. Chem. (2021). https://doi.org/10.1080/03067319.2021.1957467(2021)
28. Gupta, K.; Joshi, P.; Gusain, R.; Khatri, O.P.: Recent advances in adsorptive removal of heavy metal and metalloid ions by metal oxide-based nanomaterials. Coord. Chem. Rev. **445**, 214100 (2021)
29. Ramos-Guivar, J.A.; Flores-Cano, D.A.; Caetano Passamani, E.: Differentiating nanomaghemite and nanomagnetite and discussing their importance in arsenic and lead removal from contaminated effluents: a critical review. Nanomaterials **11**, 2310 (2021)
30. Pritchett, P.: Instability of current sheets with a localized accumulation of magnetic flux. Phys. Plasmas **22**, 062102 (2015)
31. Fadillah, G.; Yudha, S.P.; Sagadevan, S.; Fatimah, I.; Muraza, O.: Magnetic iron oxide/clay nanocomposites for adsorption and catalytic oxidation in water treatment applications. Open Chem. **18**, 1148–1166 (2020)
32. Lasheen, M.; El-Sherif, I.Y.; Sabry, D.Y.; El-Wakeel, S.; El-Shahat, M.: Adsorption of heavy metals from aqueous solution by magnetite nanoparticles and magnetite-kaolinite nanocomposite: equilibrium, isotherm and kinetic study. Desalin. Water Treat. **57**, 17421–17429 (2016)
33. Mohammed, A.A.; Isra'a, S.S.: Bentonite coated with magnetite Fe_3O_4 nanoparticles as a novel adsorbent for copper (II) ions removal from water/wastewater. Environ. Technol. Innov. **10**, 162–174 (2018)
34. Won, J.; Wirth, X.; Burns, S.E.: An experimental study of cotransport of heavy metals with kaolinite colloids. J. Hazard. Mater. **373**, 476–482 (2019)
35. de Macedo Neto, J.C.; do Nascimento, N.R.; Bello, R.H.; de Verçosa, L.A.; Neto, J.E.; da Costa, J.C.M.; Rol, F.: Kaolinite review: intercalation and production of polymer nanocomposites. Eng. Sci. **17**, 28-44 (2021)

36. Li, J.; Wen, F.; Pan, L.; Liu, Z.; Dong, Y.: Removal of radiocobalt ions from aqueous solutions by natural halloysite nanotubes. J. Radioanal. Nucl. Chem. **295**, 431–438 (2013)
37. Jin, J.; Assemi, S.; Asgar, H.; Gadikota, G.; Tran, T.; Nguyen, W.; McLennan, J.D.; Miller, J.D.: Characterization of natural consolidated halloysite nanotube structures. Minerals **11**, 1308 (2021)
38. Yuan, P.; Tan, D.; Annabi-Bergaya, F.; Yan, W.; Liu, D.; Liu, Z.: From platy kaolinite to aluminosilicate nanoroll via one-step delamination of kaolinite: effect of the temperature of intercalation. Appl. Clay Sci. **83**, 68–76 (2013)
39. Machida, S.; Gotoh, T.; Katsumata, K.-I.; Yasumori, A.: A facile method of generating aluminosilicate nanoparticles: complete fragmentation of kaolinite nanoscrolls via manual grinding. Appl. Clay Sci. **214**, 106295 (2021)
40. Abukhadra, M.R.; Bakry, B.M.; Adlii, A.; Yakout, S.M.; El-Zaidy, M.E.: Facile conversion of kaolinite into clay nanotubes (KNTs) of enhanced adsorption properties for toxic heavy metals (Zn^{2+}, Cd^{2+}, Pb^{2+}, and Cr^{6+}) from water. J. Hazard. Mater. **374**, 296–308 (2019)
41. Kuroda, Y.; Ito, K.; Itabashi, K.; Kuroda, K.: One-step exfoliation of kaolinites and their transformation into nanoscrolls. Langmuir **27**, 2028–2035 (2011)
42. Gardolinski, J.; Lagaly, G.: Grafted organic derivatives of kaolinite: II. Intercalation of primary n-alkylamines and delamination. Clay Miner. **40**, 547–556 (2005)
43. Matusik, J.; Scholtzová, E.; Tunega, D.; Rueda, E.H.: Influence of synthesis conditions on the formation of a kaolinite-methanol complex and simulation of its vibrational spectra. Clays Clay Miner. **60**, 227–239 (2012)
44. Makó, É.; Kovács, A.; Katona, R.; Kristóf, T.: Characterization of kaolinite-cetyltrimethylammonium chloride intercalation complex synthesized through eco-friend kaolinite-urea pre-intercalation complex. Colloids Surf. A **508**, 265–273 (2016)
45. Li, X.; Wang, D.; Liu, Q.; Komarneni, S.: A comparative study of synthetic tubular kaolinite nanoscrolls and natural halloysite nanotubes. Appl. Clay Sci. **168**, 421–427 (2019)
46. Yuan, P.; Tan, D.; Annabi-Bergaya, F.: Properties and applications of halloysite nanotubes: recent research advances and future prospects. Appl. Clay Sci. **112**, 75–93 (2015)
47. Andrini, L.; Toja, R.M.; Conconi, M.S.; Requejo, F.G.; Rendtorff, N.: Halloysite nanotube and its firing products: Structural characterization of halloysite, metahalloysite, spinel type silicoaluminate and mullite. J. Electron Spectrosc. Relat. Phenom. **234**, 19–26 (2019)
48. Li, X.; Liu, Q.; Cheng, H.; Komarneni, S.: High-yield production of mesoporous nanoscrolls from kaolinite by ultrasonic assisted exfoliation. Microporous Mesoporous Mater. **241**, 66–71 (2017)
49. Nakagaki, S.; Machado, G.S.; Halma, M.; dos Santos Marangon, A.A.; de Freitas Castro, K.A.D.; Mattoso, N.; Wypych, F.: Immobilization of iron porphyrins in tubular kaolinite obtained by an intercalation/delamination procedure. J. Catal. **242**, 110–117 (2006)
50. Meziane, O.; Bensedira, A.; Melia, G.; Haddaoui, N.: Preparation and characterization of intercalated kaolinite with: urea, dimethyl formamide and an alkylammonium salt using guest displacement reaction. J. Mater. Environ. Sci. **8**, 3625–3635 (2017)
51. Qu, H.; He, S.; Su, H.: Efficient preparation of kaolinite/methanol intercalation composite by using a Soxhlet extractor. Sci. Rep. **9**, 8351 (2019)
52. Xu, H.; Liu, J.; Chen, P.; Shao, G.; Fan, B.; Wang, H.; Chen, D.; Lu, H.; Zhang, R.: Preparation of magnetic kaolinite nanotubes for the removal of methylene blue from aqueous solution. J. Inorg. Organomet. Polym. Mater. **28**, 790–799 (2018)
53. Abukhadra, R.; Fadl Allah, A.: Synthesis and characterization of kaolinite nanotubes (KNTs) as a novel carrier for 5-fluorouracil of high encapsulation properties and controlled release. Inorg. Chem. Commun. **103**, 30–36 (2019)
54. Sachan, A.; Penumadu, D.: Identification of microfabric of kaolinite clay mineral using X-ray diffraction technique. Geotech. Geol. Eng. **25**, 603–616 (2007)
55. Xu, H.; Jin, X.; Chen, P.; Shao, G.; Wang, H.; Chen, D.; Lu, H.; Zhang, R.: Preparation of kaolinite nanotubes by a solvothermal method. Ceram. Int. **41**, 6463–6469 (2015)
56. Abukhadra, M.R.; Allah, A.F.: Synthesis and characterization of kaolinite nanotubes (KNTs) as a novel carrier for 5-fluorouracil of high encapsulation properties and controlled release. Inorg. Chem. Commun. **103**, 30–36 (2019)
57. Makó, É.; Kovács, A.; Antal, V.; Kristóf, T.: One-pot exfoliation of kaolinite by solvothermal cointercalation. Appl. Clay Sci. **146**, 131–139 (2017)
58. Butulija, S.; Spasojević, V.; Branković, G.; Prekajski Đorđević, M.; Radulović, T.; Zarubica, A.; Matović, B.: Synthesis, characterization and magnetic properties of spider silk coated with maghemite (γ-Fe_2O_3) nanoparticles. Mater. Lett. **314**, 131856 (2022)
59. Rodriguez, A.; Rocha, C.; Piazza, R.; Dos Santos, C.; Morales, M.; Faria, F.; Iqbal, M.Z.; Barbosa, L.; Chaves, Y.; Mariuba, L.: Synthesis, characterization and applications of maghemite beads functionalized with rabbit antibodies. Nanotechnology **29**, 365701 (2018)
60. Saikia, B.J.; Parthasarathy, G.: Fourier transform infrared spectroscopic characterization of kaolinite from Assam and Meghalaya, Northeastern India. J. Mod. Phys **1**, 206–210 (2010)
61. Dewi, R.; Agusnar, H.; Alfian, Z.: Characterization of technical kaolin using XRF, SEM, XRD, FTIR and its potentials as industrial raw materials. J. Phys. Conf. Ser. **1116**, 042010 (2018)
62. Kumar, A.; Lingfa, P.: Sodium bentonite and kaolin clays: comparative study on their FT-IR, XRF, and XRD. Mater. Today Proc. **22**, 737–742 (2020)
63. Sohrabijam, Z.; Zamanian, A.; Saeidifar, M.; Nouri, A.: Preparation and characterization of superparamagnetic chitosan coated maghemite (γ-Fe_2O_3) for gene delivery. Procedia Mater. Sci. **11**, 282–286 (2015)
64. Shikuku, V.O.; Mishra, T.: Adsorption isotherm modeling for methylene blue removal onto magnetic kaolinite clay: a comparison of two-parameter isotherms. Appl. Water Sci. **11**, 103 (2021)
65. Jain, M.; Yadav, M.; Kohout, T.; Lahtinen, M.; Garg, V.K.; Sillanpää, M.: Development of iron oxide/activated carbon nanoparticle composite for the removal of Cr (VI), Cu (II) and Cd (II) ions from aqueous solution. Water Resour. Ind. **20**, 54–74 (2018)
66. Abdelbasir, S.M.; El-Shewaikh, A.M.; El-Sheikh, S.M.; Ali, O.I.: Novel modified chitosan nanocomposites for Co(II) ions removal from industrial wastewater. J. Water Process Eng. **41**, 102008 (2021)
67. Saraeian, A.; Hadi, A.; Raji, F.; Ghassemi, A.; Johnson, M.: Cadmium removal from aqueous solution by low-cost native and surface modified Sorghum x drummondii (Sudangrass). J. Environ. Chem. Eng. **6**, 3322–3331 (2018)
68. Naushad, M.; Alqadami, A.A.; Al-Kahtani, A.A.; Ahamad, T.; Awual, M.R.; Tatarchuk, T.: Adsorption of textile dye using para-aminobenzoic acid modified activated carbon: kinetic and equilibrium studies. J. Mol. Liq. **296**, 112075 (2019)
69. Bouhamed, F.; Elouear, Z.; Bouzid, J.: Adsorptive removal of copper (II) from aqueous solutions on activated carbon prepared from Tunisian date stones: equilibrium, kinetics and thermodynamics. J. Taiwan Inst. Chem. Eng. **43**, 741–749 (2012)
70. Freundlich, H.: Over the adsorption in solution. J. Phys. Chem. **57**, 385– 471 (1906)
71. Hanaor, D.A.; Ghadiri, M.; Chrzanowski, W.; Gan, Y.: Scalable surface area characterization by electrokinetic analysis of complex anion adsorption. Langmuir **30**, 15143–15152 (2014)

72. Munjur, H.M.; Hasan, M.N.; Awual, M.R.; Islam, M.M.; Shenashen, M.; Iqbal, J.: Biodegradable natural carbohydrate polymeric sustainable adsorbents for efficient toxic dye removal from wastewater. J. Mol. Liq. **319**, 114356 (2020)
73. Günay, A.; Arslankaya, E.; Tosun, İ: Lead removal from aqueous solution by natural and pretreated clinoptilolite: adsorption equilibrium and kinetics. J. Hazard. Mater. **146**, 362–371 (2007)
74. Abatal, M.; Olguin, M.; Anastopoulos, I.; Giannakoudakis, D.A.; Lima, E.C.; Vargas, J.; Aguilar, C.: Comparison of heavy metals removal from aqueous solution by Moringa oleifera leaves and seeds. Coatings **11**, 508 (2021)
75. Shahmohammadi-Kalalagh, S.; Babazadeh, H.; Nazemi, A.; Manshouri, M.: Isotherm and kinetic studies on adsorption of Pb, Zn and Cu by kaolinite. Caspian J. Environ. Sci. **9**, 243–255 (2011)
76. Mohammadnezhad, G.; Soltani, R.; Abad, S.; Dinari, M.: A novel porous nanocomposite of aminated silica MCM-41 and nylon-6: Isotherm, kinetic, and thermodynamic studies on adsorption of Cu (II) and Cd (II). J. Appl. Polym. Sci. **134**, 45383 (2017)
77. Yuh-Shan, H.: Citation review of Lagergren kinetic rate equation on adsorption reactions. Scientometrics **59**, 171–177 (2004)
78. Weber, W.J.; Morris, J.C.: Kinetics of adsorption on carbon from solution. J. Sanit. Eng. Div. **89**, 31–59 (1963)
79. Kubra, K.T.; Salman, M.S.; Hasan, M.N.; Islam, A.; Hasan, M.M.; Awual, M.R.: Utilizing an alternative composite material for effective copper (II) ion capturing from wastewater. J. Mol. Liq. **336**, 116325 (2021)
80. Xu, P.; Zeng, G.M.; Huang, D.L.; Lai, C.; Zhao, M.H.; Wei, Z.; Li, N.J.; Huang, C.; Xie, G.X.: Adsorption of Pb (II) by iron oxide nanoparticles immobilized Phanerochaete chrysosporium: equilibrium, kinetic, thermodynamic and mechanisms analysis. Chem. Eng. J. **203**, 423–431 (2012)
81. Gong, J.-L.; Wang, X.-Y.; Zeng, G.-M.; Chen, L.; Deng, J.-H.; Zhang, X.-R.; Niu, Q.-Y.: Copper (II) removal by pectin–iron oxide magnetic nanocomposite adsorbent. Chem. Eng. J. **185**, 100–107 (2012)
82. Sen, T.K.; Sarzali, M.V.: Removal of cadmium metal ion (Cd^{2+}) from its aqueous solution by aluminium oxide (Al_2O_3): A kinetic and equilibrium study. Chem. Eng. J. **142**, 256–262 (2008)
83. Sari, A.; Tuzen, M.: Cd (II) adsorption from aqueous solution by raw and modified kaolinite. Appl. Clay Sci. **83**, 63–72 (2014)
84. Adebowale, K.O.; Unuabonah, E.I.; Olu-Owolabi, B.I.: Kinetic and thermodynamic aspects of the adsorption of Pb^{2+} and Cd^{2+} ions on tripolyphosphate-modified kaolinite clay. Chem. Eng. J. **136**, 99–107 (2008)
85. Kahkha, M.R.R.; Kaykhaii, M.; Kahkha, B.R.; Khosravi, H.; Tohidlou, E.: Simultaneous removal of heavy metals from wastewater using modified sodium montmorillonite nanoclay. Anal. Sci. **36**, 1039–1043 (2020)
86. Li, R.; Wang, J.J.; Gaston, L.A.; Zhou, B.; Li, M.; Xiao, R.; Wang, Q.; Zhang, Z.; Huang, H.; Liang, W.: An overview of carbothermal synthesis of metal–biochar composites for the removal of oxyanion contaminants from aqueous solution. Carbon **129**, 674–687 (2018)
87. Bhattacharyya, K.G.; Gupta, S.S.: Adsorptive accumulation of Cd (II), Co (II), Cu (II), Pb (II), and Ni (II) from water on montmorillonite: influence of acid activation. J. Colloid Interface Sci. **310**, 411–424 (2007)
88. Awual, M.R.: A facile composite material for enhanced cadmium(II) ion capturing from wastewater. J. Environ. Chem. Eng. **7**, 103378 (2019)
89. Hasan, M.N.; Salman, M.S.; Islam, A.; Znad, H.; Hasan, M.M.: Sustainable composite sensor material for optical cadmium (II) monitoring and capturing from wastewater. Microchem. J. **161**, 105800 (2021)
90. Shahat, A.; Kubra, K.T.; Salman, M.S.; Hasan, M.N.; Hasan, M.M.: Novel solid-state sensor material for efficient cadmium(II) detection and capturing from wastewater. Microchem. J. **164**, 105967 (2021)